THE ASTROPHYSICAL JOURNAL, 411:756–760, 1993 July 10

THE RADIO STRUCTURE OF SUPERNOVA REMNANT 0540−693

R. N. MANCHESTER, L. STAVELEY-SMITH, AND M. J. KESTEVEN
Australia Telescope National Facility, CSIRO, PO Box 76, Epping, NSW 2121, Australia
Received 1992 October 26; accepted 1992 December 16

ABSTRACT

We present an Australia Telescope Compact Array multifrequency study of the supernova remnant 0540−693 which is the youngest known remnant, after SN 1987A, in the Large Magellanic Cloud. The radio observations reveal that it consists of a central synchrotron nebula of diameter 1.4 pc which is powered by the 50 ms pulsar PSR B0540−69, and a nearly circular low-surface brightness annulus of diameter 17.5 pc. The central nebula has a flatter spectrum than the annular emission and is the radio counterpart of the synchrotron nebula previously detected at optical and X-ray wavelengths. Its properties are very similar to those of the Crab Nebula. The annular emission is similar to other young supernova remnant shells and is generated by the interaction of the supernova ejecta with the circumstellar medium.

Subject headings: ISM: individual (SNR 0540 693) — pulsars: individual (PSR B0540−69) — radio continuum: interstellar — supernova remnants

1. INTRODUCTION

The radio source 0540−693, located in the Large Magellanic Cloud, was first cataloged as a discrete radio source by Le Marne (1968) and as a supernova remnant (SNR), based on its spectral index, by Mathewson & Clarke (1973). The object was detected as an X-ray source by Long & Helfand (1979) and at optical wavelengths as an oxygen-rich annulus of diameter ∼8″ by Mathewson et al. (1980), thus confirming its identification as an SNR. X-ray spectral observations by Clark et al. (1982) showed that the X-ray emission was nonthermal and hence probably from a pulsar-driven synchrotron nebula. This hypothesis received dramatic confirmation with the discovery at X-ray wavelengths of a 50 ms pulsar at the center of the nebula by Seward, Harnden, & Helfand (1984). The X-ray observations showed that the pulsar was spinning down rapidly, with a characteristic age, $P/(2\dot{P})$, of only 1660 yr. This, together with the unresolved nature of the X-ray synchrotron nebula and the detection of a centrally brightened optical synchrotron nebula of half-power diameter ∼4″ by Chanan, Helfand, & Reynolds (1984) showed that SNR 0540−693 is a very close analogue of the Crab Nebula.

The pulsar was subsequently detected at optical wavelengths by Middleditch & Pennypacker (1985) and radio wavelengths by Manchester et al. (1993). Optical and X-ray pulse timing measurements (Manchester & Peterson 1989; Nagase et al. 1990; Gouiffes, Finley, & Ögelman 1992) show that the braking index for the pulsar is 2.01 ± 0.02, giving a spin-down age (from zero period) of 3260 yrs. However, measurements of the expansion velocity of the optical spectral-line region, together with its observed diameter of 8″, show that, for an assumed distance of 55 kpc, the SNR age, τ, is 760 ± 100 yr (Reynolds 1985; Kirshner et al. 1989). The age uncertainty is dominated by the unknown acceleration of the ejecta by the pulsar and/or deceleration by interaction with the surrounding interstellar medium. For an age of 760 yrs and a constant braking index of 2.01, the period of the pulsar at birth was about 38.7 ms. Recently, Caraveo et al. (1992) have obtained high-resolution optical images of the SNR and derived an improved position for the pulsar.

Prior to the present observations, the highest resolution radio observations were made using the Molonglo Observatory Synthesis Telescope (MOST) which, at the operating frequency of 843 MHz, has a half-power beamwidth of 44″ (Mills et al. 1984). These observations just resolved the remnant[1] and gave a flux density of 1055 mJy. In this paper, we report on observations made using the Compact Array of the Australia Telescope at frequencies near 5 GHz giving an angular resolution 16 times greater. These resolve the radio remnant into a central pulsar-driven component and a surrounding shell emission which has a diameter of ∼65″. Compact Array observations at 1.5 GHz show that the central source has a flatter spectrum than the shell emission.

2. OBSERVATIONS AND ANALYSIS

The 5 GHz observations were made using the 3 km east-west baseline of the Australia Telescope Compact Array in four sessions in 1990: May 6, May 19, June 3, and August 19. Except for the second session, the five 22 m antennas of the 3 km array were used and the observations were of duration ∼12 hr. For the second session, only four antennas were available and the observation duration was ∼9 hr. The array configuration was different for each session, giving 36 different physical baselines in the range 31–3000 m. The actual observation frequency was timed-shared between 4.786 and 5.814 GHz further improving the coverage of the spatial frequency plane. Receiver system temperatures were ∼55 K. The 1.5 GHz observations (central frequency 1.472 GHz) were made on 1991 September 9 using all six antennas of the Compact Array. This gave 15 baselines in the range 153–6000 m. The observation duration was 7 hr and receiver system temperatures were ∼45 K.

For all observations, the total bandwidth of 128 MHz was split into 32 frequency channels, each of 4 MHz, and the correlator integration time was 10 s. Flux densities were referred to PKS B1934−638 which was assumed to have flux densities of 16.1, 6.3, and 4.8 Jy at 1.472, 4.786, and 5.814 GHz, respectively. Three nearby unresolved sources, PKS B0454−810,

[1] The extended skirt around the central source in the image of Mills et al. (1984) was subsequently shown to be an artifact of the data processing (A. J. Turtle & B. Y. Mills, private communication, 1990).

PKS B0530−727, and PKS B0637−752[2] were observed for 3–5 minutes every 15–20 minutes as secondary calibrators for both flux density and phase. The VLBI positions for these sources (Harvey et al. 1992; Russell et al. 1992) agree to better than 0.″2 with the position of the optical identification.

Images were created and processed using the Astronomical Image Processing System (AIPS) running on a Convex C220 computer and Sun workstations. For the 5 GHz observations, the data were averaged over the 128 MHz bandwidth, edited, calibrated, transformed into the image plane using a pixel size of 1″ × 1″, and CLEANed. At this declination, the synthesised beam is almost circular and has a half-power width of 2.″7. The final image is shown in Figure 1. Owing to the proximity of strong radio sources, in particular, the 30 Doradus complex, the rms background noise, 0.2 mJy beam^{-1}, is larger than expected on the basis of the system parameters. The 1.5 GHz data were imaged in a similar way except that visibilities for each 4 MHz channel were separately transformed to avoid smearing of the beam due to the large fractional bandwidth. The final image, shown in Figure 2, has large sidelobes owing to the relatively poor spatial frequency coverage of the observations.

At 5 GHz (Fig. 1), the central source is clearly resolved. For an elliptical Gaussian shape, its deconvolved half-power width is 5.″3 × 4.″8 with an uncertainty of ±0.″3 in each axis and with the major axis at a position angle of 56° ± 30°. At the assumed distance of 55 kpc, the corresponding linear dimensions are 1.4 × 1.3 pc. The centroid positions (J2000) from the 5 and 1.5 GHz images are given in Table 1. Although the boundary of the shell emission is somewhat irregular, it is contained within a circle of diameter 65″ corresponding to a linear diameter of ~17.5 pc. The center of this circle lies within a few arcseconds of the peak of the central source.

[2] PKS B0637−752 has an extended low frequency halo and was not used for the 1.5 GHz observations.

TABLE 1

POSITIONS OF CENTRAL FEATURES

Parameter	R.A. (J2000)	Decl. (J2000)	Reference
Radio (5 GHz)	$05^h40^m11^s.30 \pm 0^s.03$	$-69°19'53.''9 \pm 0.''1$	1
Radio (1.5 GHz)	$05^h40^m11^s.27 \pm 0^s.11$	$-69°19'53.''7 \pm 0.''3$	1
Optical ([O III])	$05^h40^m11^s$	$-69°19'58''$	2
PSR (X-ray)	$05^h40^m11^s.0 \pm 0^s.7$	$-69°19'57.''4 \pm 2.''0$	3
PSR (Optical)	$05^h40^m10^s.99 \pm 0^s.18$	$-69°19'55.''1 \pm 0.''5$	4

REFERENCES.—(1) This work; (2) Mathewson et al. 1983; (3) Seward, Harnden, & Helfand 1984; (4) Caraveo et al. 1992.

Determination of the flux density of the central source is complicated by the presence of underlying shell emission. The level of the underlying emission was estimated by integrating within an annular region of width 2″ surrounding and just outside the wings of the central source. After subtraction of this base level, the integrated flux density of the central source was 59 mJy at 5 GHz and 79 mJy at 1.5 GHz. A similar analysis yielded flux densities of 520 and 740 mJy for the whole source at 5 and 1.5 GHz, respectively. Uncertainties in these numbers are difficult to estimate but are probably less than 10%.

3. DISCUSSION

As Figure 1 shows, SNR 0540−693 is the clearest example known of an SNR containing a known pulsar, a central pulsar-driven nebula or plerion and surrounding shell emission. Based on its measured diameter of 65″, the shell emission has a mean surface brightness at 408 MHz of 1.6×10^{-19} W m^{-2} Hz^{-1} sr^{-1}. This value is within 20% of the best-fit value for Galactic shell remnants derived by Clark & Caswell (1976), confirming the shell nature of this emission. The shell emission

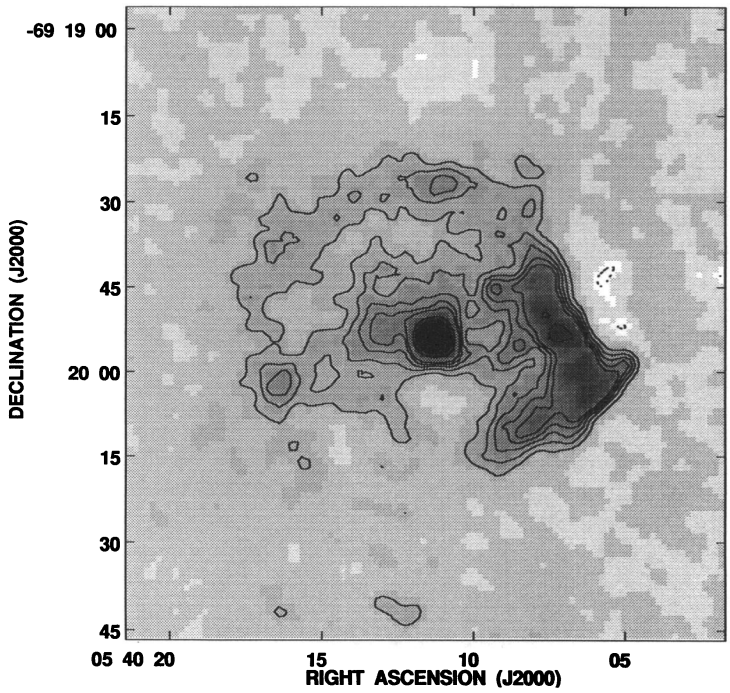

FIG. 1.—Radio image of SNR 0540−693 at 5 GHz from four 12 hr (nominal) observations with the 3 km Australia Telescope Compact Array. The synthesized beam is nearly circular and of half-power width 2.″7. Contour levels are −0.5 (*dashed line*), 0.5, 1.0, 1.5, 2.0, 2.5, 5.0, 7.5, and 10.0 mJy beam^{-1}.

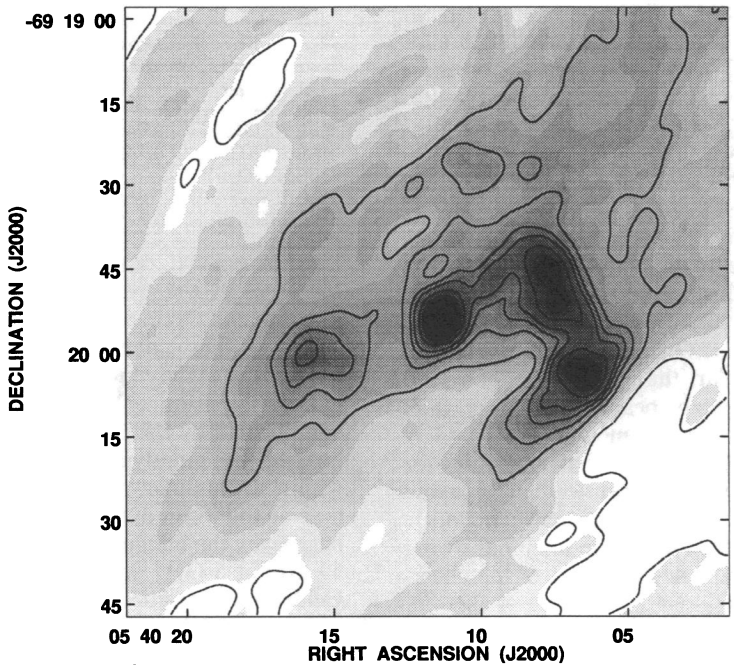

FIG. 2.—Radio image of SNR 0540−693 at 1.5 GHz from a 7 hr observation with the 6 km Australia Telescope Compact Array. The synthesized beam half-power width is ~5″ and the contour levels are −2 (*dashed line*), 2, 4, 6, 8, 12, 16, 20, 30 and 40 mJy beam^{-1}.

is weak in the southern quadrant whereas in the west it is strong with a very steep outer edge. This region of strong emission coincides with weak [O III] filamentary structure (Mathewson et al. 1983) and weak extensions of the X-ray emission (Seward 1989), confirming that these emission regions are associated with the SNR. There is a prominent indentation of the outer boundary of the shell just north of west, suggesting that expansion in this direction may be impeded by a high-density cloud. The CO survey of the Large Magellanic Cloud by Cohen et al. (1988) has a hint of a concentration just west of SNR 0540−693 and the H II complex DEM 269 (Davies, Elliott, & Meaburn 1976) lies slightly south. Such interactions do not, however, appear to be responsible for the enhanced emissivity in this region. The bright region stops short of the end of the indentation on the north side and extends below it on the south side. Recent observations of the G308.8−0.1–PSR 1338−62 association (Caswell et al. 1992; Kaspi et al. 1992) suggest that pulsars may inject relativistic particles into portions of the shell creating a region of enhanced emission. It is possible that such injection is also responsible for the bright region in SNR 0540−693.

The size and shape of the central optical and radio continuum sources are very similar, whereas the [O III] emission is clearly annular and of larger radius. The [O III] emission is from supernova ejecta which are probably shock-excited and have a present maximum expansion velocity of ~1400 km s^{-1} (Kirshner et al. 1989; Chevalier & Fransson 1992). The radio shell emission has a diameter ~8 times that of the [O III] ring and has clearly expanded much faster than the bulk of the ejecta. If we adopt 760 yr as the age of the nebula, then the average expansion velocity of the shell is 10,800 km s^{-1}. Since the shell emission is attributed to acceleration of relativistic particles by the "fast shock" preceding the highest velocity ejecta, this high velocity implies that the maximum velocity of the ejecta was at least 10,800 km s^{-1}. The very presence of the radio shell shows that there has been deceleration, so the initial maximum velocity of ejection must have been significantly greater.

Figure 3 shows flux densities from the 5 and 1.5 GHz observations plotted as a function of frequency, along with other measured values for the remnant as a whole. Except for the 14.7 GHz point (Milne, Caswell, & Haynes 1980), the whole-source spectrum is well fitted by a power law with spectral index −0.41, typical of SNRs. The high-frequency point is probably affected by background thermal emission. It is clear from Figures 1 and 2 that the spectrum of the central source is flatter than that of the shell and this is quantified in Figure 3. The spectral index derived from these two flux densities is −0.25 with an uncertainty of the order of 0.1. This is close to the value of −0.30 derived for the Crab Nebula (Baars et al. 1977) and is typical of pulsar-driven nebulae.

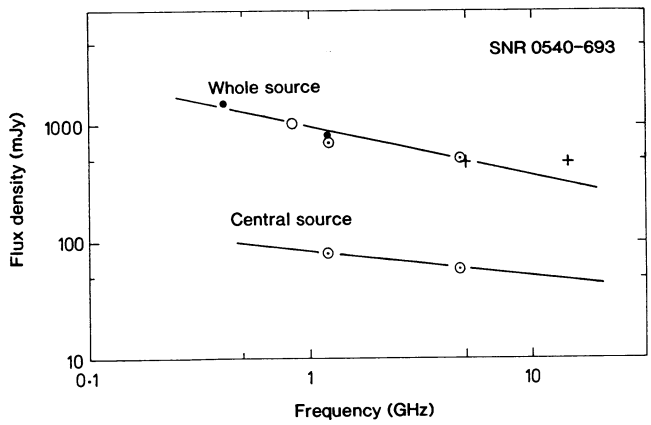

FIG. 3.—Radio frequency spectra of SNR 0540−693 and of the central souce. Flux densities are from Mills, Turtle, & Watkinson (1978, ●); Milne, Caswell, & Haynes (1980, +); Mills et al. (1984, ○); and this paper (⊙).

At optical and X-ray wavelengths, the spectral index of the synchrotron nebula is close to −0.8 (Clark et al. 1982; Chanan, Helfand, & Reynolds 1984). This is steeper than the radio spectrum by 0.5 in spectral index, exactly as expected if the nebula is driven by a source of relativistic electrons with a constant power-law energy spectrum going as $E^{-2.6}$, and the lifetime of the relativistic electrons against synchrotron losses for the high-energy radiation is less than the nebular lifetime. Extrapolation of the radio and high-energy spectra shows that the break frequency between the two regimes must be close to 2×10^{13} Hz. The synchrotron lifetime is given by $\tau_s \approx 6 \times 10^{11} B^{-3/2} \nu^{-1/2}$, where τ_s is in seconds, B is the nebular magnetic field in Gauss, and ν is the synchrotron frequency in Hertz. At the break frequency, τ_s is the nebular lifetime, so we derive a value of 3.2×10^{-4} $(\tau/760 \text{ yr})^{-2/3}$ G for the nebular magnetic flux density.

The nebular synchrotron luminosity is dominated by the high-frequency radiation and is about equal to the pulsar spin-down luminosity, 1.5×10^{38} ergs s^{-1}, if the nebular spectrum extends as far 10^{23} Hz with a constant spectral index of −0.8. Below the spectral break, the total synchrotron luminosity is only $\sim 5 \times 10^{35}$ ergs s^{-1}. However, the total energy content of the relativistic electrons responsible for the synchrotron emission is dominated by the low-energy part of the spectrum and is $\sim 1.5 \times 10^{-9}$ ergs cm^{-3}, corresponding to $\sim 6 \times 10^{46}$ ergs for the whole nebula. For $B = 3.2 \times 10^{-4}$ G, the magnetic energy density, $B^2/8\pi$, is ~3 times the energy density of the relativistic electrons. The total magnetic and relativistic electron content is ~4% of the integrated spin-down luminosity of the pulsar over the past 760 yr, assuming a constant pulsar braking index of 2.0. Most of the pulsar luminosity is probably lost as high-energy synchrotron radiation, but some may go into expansion of the nebula or acceleration of relativistic ions.

As listed in Table 1, the best position for the pulsar (Caraveo et al. 1992) lies ~1.″5 west and 1.″2 south, or somewhat more than twice the estimated error in each coordinate, of the radio centroid. The uncertainty in alignment of the radio and optical reference frames is believed to be less than 0.″2, although the 0.″5 offset of the radio SNR 1987A from the optical SN 1987A position (Staveley-Smith et al. 1992) suggests that the error may be greater. The lifetime of the radio-emitting synchrotron electrons is much greater than the age of the nebula, so, if we assume that the pulsar luminosity has been roughly constant since birth (Chevalier & Fransson 1992) and that the 1.″9 offset is genuine, the pulsar has moved twice this distance in 760 yr, corresponding to a proper motion of ~5 mas yr^{-1}. The images of Caraveo et al. suggest that the pulsar lies ~0.″5 southwest of the center of the optical synchrotron nebula. Since the optical synchrotron electrons have a lifetime of ~120 yr, a similar proper motion toward the southwest is implied. At a distance of 55 kpc, this proper motion corresponds to a transverse velocity of ~1200 km s^{-1}. This is high, but not unprecedented, for observed pulsar transverse velocities (Harrison, Lyne & Anderson 1993; Frail & Kulkarni 1991; Manchester et al. 1991).

SNR 0540−693 and its pulsar, PSR B0540−69, are clearly very similar to the Crab Nebula and its pulsar. Table 2 summarizes the comparison between the two systems. Continuum spectra from radio to gamma ray wavelengths are compared in Figure 4. At optical and X-ray wavelengths, the SNR 0540−693 central nebula has a somewhat flatter spectrum than the Crab Nebula and about one-third of its luminosity. This is in the same ratio as the pulsar spin-down luminosities.

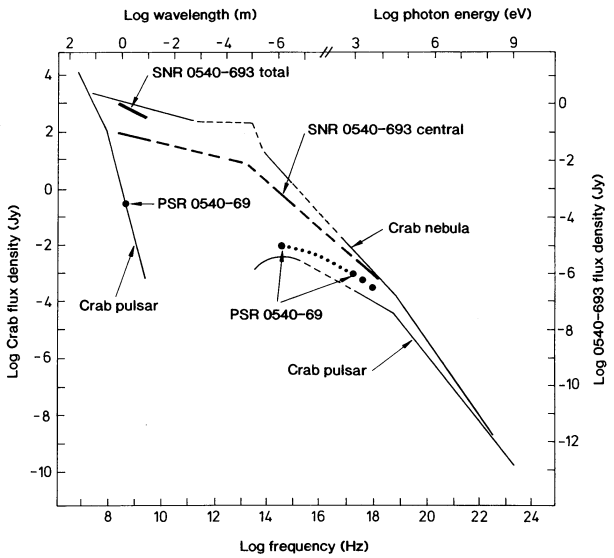

FIG. 4.—Continuum spectra from low radio to gamma-ray frequencies for the Crab Nebula and pulsar and for SNR 0540−693 and PSR B0540−69. The flux density scales are adjusted so that luminosities for the two systems may be directly compared. Data for the Crab Nebula and pulsar are from the compilation by Manchester & Taylor (1977). Flux densities for SNR 0540−693 are from this paper, Chanan, Helfand, & Reynolds (1984) and Clark et al. (1982) and for PSR B0540−69 are from Manchester et al. (1992), Middleditch, Pennypacker, & Burns (1987), and Seward (1989).

Within the uncertainties, the radio spectral index of the central nebula in SNR 0540−693 is identical to that of the Crab Nebula and both spectra have a break at $\sim 10^{13}$ Hz. The SNR 0540−693 central nebula is about half the linear size of the Crab Nebula and hence about one-eighth of the volume, so its volume emissivity is about a factor of 2 higher than that of the Crab Nebula.

The properties of the two pulsars are also broadly similar, although there are large differences in detailed properties such as pulse shape. The radio detection of PSR B0540−69 lies on the Crab pulsar spectrum, although the exact agreement is surely fortuitious. PSR B0540−69 is somewhat brighter than the Crab pulsar at optical and X-ray frequencies. The pulsar has not been detected above a few keV, but the energy arguments given above suggest that the spectrum must steepen at higher energies as it does in the Crab pulsar.

In summary, we have shown SNR 0540−693 to be a composite remnant, with a central bright feature receiving its exci-

TABLE 2

COMPARISON OF THE SNR 0540−693 AND CRAB SYSTEMS

Parameter	0540−693	Crab
Age (yr)	~760	~938
Radio plerion half-power width (pc)	1.4 × 1.3	3.5 × 2.3
Radio shell diameter (pc)	17.5	...
Spectral indices:		
Radio shell	−0.41	...
Radio plerion	−0.25	−0.30
Optical/X-ray plerion	−0.8	−1.0
Plerion luminosity (to 4 keV) (ergs s^{-1})	2×10^{37}	6×10^{37}
Pulsar period (ms)	50.3	33.3
Pulsar braking index	2.01	2.51
Pulsar initial period (ms)	38.7	19.5
Pulsar spin-down luminosity (ergs s^{-1})	1.5×10^{38}	4.5×10^{38}

tation directly from PSR B0540−69. It is a very close analog to the Crab Nebula. The more extended emission has the morphology and surface brightness typical of shell SNRs and is undoubtedly due to interaction of rapidly expanding ejecta with the surrounding interstellar medium. There are significant variations in surface brightness around the shell which appear to be determined by factors other than the density of the surrounding medium.

REFERENCES

Baars, J. W. M., Genzel, R., Pauliny-Toth, I. I. K., & Witzel, A. 1977, A&A, 61, 99
Caraveo, P. A., Bignami, G. F., Mereghetti, S., & Mombelli, M. 1992, ApJ, 395, L103
Caswell, J. L., Kesteven, M. J., Stewart, R. T., Milne, D. K., & Haynes, R. H. 1992, ApJ, 399, L151
Chanan, G. A., Helfand, D. J., & Reynolds, S. P. 1984, ApJ, 287, L23
Chevalier, R. A., & Fransson, C. 1992, ApJ, 395, 540
Clark, D. H., & Caswell, J. L. 1976, MNRAS, 174, 267
Clark, D. H., Tuohy, I. R., Long, K. S., Szymkowiak, A. E., Dopita, M. A., Mathewson, D. S., & Culhane, J. L. 1982, ApJ, 255, 440
Cohen, R. S., Dame, T. M., Garay, G., Montani, J., Rubio, M., & Thaddeus, P. 1988, ApJ, 331, L95
Davies, R. D., Elliott, K. H., & Meaburn, J. 1976, MmRAS, 81, 89
Frail, D. A., & Kulkarni, S. R. 1991, Nature, 352, 785
Gouiffes, C., Finley, J. P., & Ögelman, H. 1992, ApJ, 394, 581
Harrison, P. A., Lyne, A. G., & Anderson, B. 1993, MNRAS, In Press
Harvey, B. R., Jauncey, D. L., White, G. L., Nothnagel, A., Nicolson, G. D., Reynolds, J. E., Morabito, D. D., & Bartel, N. 1992, AJ, 103, 229
Kaspi, V. M., Manchester, R. N., Johnston, S., Lyne, A. G., & D'Amico, N. 1992, ApJ, 399, L155
Kirshner, R. P., Morse, J. A., Winkler, P. F., & Blair W. P. 1989, ApJ, 342, 260
Le Marne, A. E. 1968, MNRAS, 139, 461
Long, K. S., & Helfand, D. J. 1979, ApJ, 234, L77
Manchester, R. N., Kaspi, V. M., Johnston, S., Lyne, A. G., & D'Amico, N. 1991, MNRAS, 253, 7P
Manchester, R. N., Mar, D., Lyne, A. G., Kaspi, V. M., & Johnston, S. 1993, ApJ, 403, L29
Manchester, R. N., & Peterson, B. A. 1989, ApJ, 342, L23
Manchester, R. N., & Taylor, J. H. 1977, Pulsars (San Francisco: Freeman)
Mathewson, D. S., & Clarke, J. N. 1973, ApJ, 180, 725
Mathewson, D. S., Dopita, M. A., Tuohy, I. R., & Ford, V. L. 1980, ApJ, 242, L73
Mathewson, D. S., Ford, V. L., Dopita, M. A., Tuohy, I. R., Long, K. S., & Helfand, D. J. 1983, ApJS, 51, 345
Middleditch, J., & Pennypacker, C. 1985, Nature, 313, 659
Middleditch, J., Pennypacker, C. R., & Burns, M. S. 1987, ApJ, 315, 142
Mills, B. Y., Turtle, A. J., Little, A. G., & Durdin, J. M. 1984, Australian J. Phys., 37, 321
Mills, B. Y., Turtle, A. J., & Watkinson, A. 1978, MNRAS, 185, 263
Milne, D. K., Caswell, J. L., & Haynes, R. F. 1980, MNRAS, 191, 469
Nagase, F., Deeter, J., Lewis, W., Dotani, T., Makino, F., & Mitsuda, K. 1990, ApJ, 351, L13
Reynolds, S. P. 1985, ApJ, 291, 152
Russell, J. L., et al. 1992, AJ, 103, 2090
Seward, F. 1989, Space Sci. Rev., 49, 385
Seward, F. D., Harnden, F. R., & Helfand, D. J. 1984, ApJ, 287, L19
Staveley-Smith, L., et al. 1992, Nature, 355, 147